Nonlocal effects in inhomogeneous flows of soft athermal disks

Saitoh, Kuniyasu; Tighe, Brian P.

DOI
10.1103/PhysRevLett.122.188001

Publication date
2019

Document Version
Final published version

Published in
Physical Review Letters

Nonlocal Effects in Inhomogeneous Flows of Soft Athermal Disks

Kuniyasu Saitoh[1,2,*] and Brian P. Tighe[3]
[1]Research Alliance Center for Mathematical Sciences, Tohoku University, 2-1-1 Katahira, Aoba-ku, Sendai 980-8577, Japan
[2]WPI-Advanced Institute for Materials Research, Tohoku University, 2-1-1 Katahira, Aoba-ku, Sendai 980-8577, Japan
[3]Delft University of Technology, Process and Energy Laboratory, Leeghwaterstraat 39, 2628 CB Delft, The Netherlands

(Received 17 July 2018; published 6 May 2019)

We numerically investigate nonlocal effects on inhomogeneous flows of soft athermal disks close to but below their jamming transition. We employ molecular dynamics to simulate Kolmogorov flows, in which a sinusoidal flow profile with fixed wave number is externally imposed, resulting in a spatially inhomogeneous shear rate. We find that the resulting rheology is strongly wave-number-dependent, and that particle migration, while present, is not sufficient to describe the resulting stress profiles within a conventional local model. We show that, instead, stress profiles can be captured with nonlocal constitutive relations that account for gradients to fourth order. Unlike nonlocal flow in yield stress fluids, we find no evidence of a diverging length scale.

DOI: 10.1103/PhysRevLett.122.188001

Predictive descriptions of the rheology of soft athermal particles, e.g., emulsions, foams, colloidal suspensions, and granular materials, are frequently needed in the context of food, pharmaceutical, personal care products, and other process technologies [1]. Recently, physicists have studied the constitutive relations of these out-of-equilibrium systems in the context of jamming or yielding transitions [2–10]. However, nearly all effort to date has addressed homogeneously flowing systems, and the resulting local constitutive relations [11], even if they are generalized to tensorial forms [12], are blind to so-called nonlocal effects [13] that are relevant to spatially inhomogeneous flows of disordered materials [14,15].

Phenomenologically, nonlocality in flow refers to constitutive relations that are sensitive to spatial gradients in the shear rate. In dense amorphous matter, the effect is presumed to result from plastic events triggered by distant stress fluctuations [16–21]. In recent years, there has been substantial interest in the nonlocal continuum model of Bocquet and co-workers [22] and several related models [23–27]. They take the usual local constitutive relation, determined under homogeneous flow conditions, and introduce it as a source term in a diffusion equation for the fluidity (inverse viscosity). A so-called "cooperativity length" is required to quantify the range of nonlocal effects. These models successfully describe inhomogeneous flow profiles in emulsions [28,29], foams [30], and granular materials [23–26,31] under conditions where local models fail dramatically.

Despite these successes, important questions remain regarding how and when nonlocal effects are significant. The original fluidity model incorporated a cooperativity length that vanishes as the volume fraction ϕ approaches the jamming volume fraction ϕ_J from above [22]. In sharp contrast, more recent efforts call for a length scale that diverges at a critical stress [16,23–27]. Hence, while the concept of nonlocality does not require a yield stress, these approaches suggest a relation. De Cagny *et al.* probed granular suspensions without a yield stress and found that velocity profiles can also be fit with the fluidity model, albeit with a cooperativity length proportional to the rheometer's gap width [32]. They argued the length scale is merely a proxy for particle migration effects, and showed that a local model can describe the profiles if one accounts for spatial variations in the viscosity. Hence, the added value of nonlocal models *below* jamming remains uncertain.

In this Letter, we study nonlocal effects in "Kolmogorov flow," in which the system flows steadily under forcing that varies sinusoidally in space. This method builds on prior work in liquids [33], granular materials [34,35], and foams and emulsions [36]. We simulate dense systems of soft, viscous, athermal disks [37], the canonical model of jamming. Prior studies of this system have focused on homogeneous flows, i.e., zero wave number, and have evidenced a sensitive (critical) dependence of the homogeneous flow curves on both the proximity to jamming, $\Delta\phi = \phi_J - \phi$, and the shear rate $\dot{\gamma}$ [2–4]. From our own simulations of simple shear flows, we have verified that both the shear stress and normal stress, i.e., $\sigma^L_{xy} = \eta_s(\phi,\dot{\gamma})\dot{\gamma}$ and $\sigma^L_{yy} = \eta_c(\phi,\dot{\gamma})\dot{\gamma}$, can be described with the viscosity,

$$\eta_o(\phi,\dot{\gamma}) = \begin{cases} \bar{\eta}_o(\dot{\gamma}^{a_o} + c_o\Delta\phi^{b_o})^{-1} & (\phi < \phi_J) \\ \sigma_o(\phi)\dot{\gamma}^{-1} + \bar{\eta}_o\dot{\gamma}^{-a_o} & (\phi > \phi_J) \end{cases} \quad (1)$$

($o = s, c$), where we summarize the yield stress $\sigma_o(\phi)$ and fitting parameters $\bar{\eta}_o$, a_o, b_o, and c_o, in the Supplemental

Material [38]. Our focus here is primarily on the case without a yield stress, $\phi < \phi_J \simeq 0.842$. We find (i) constitutive relations depend on gradients of the strain rate, (ii) particle migration modifies the predictions of local models, but cannot account for the observed stress profiles, (iii) nonlocal models correctly capture the resulting stress profiles, while (iv) the cooperativity length remains small for all simulated flow parameters.

Numerical methods.—We use molecular dynamics (MD) simulations of soft athermal disks. First, we randomly distribute an equal number of small and large disks (diameters d_S and $d_L = 1.4d_S$) in a $L \times L$ periodic box. The total number of disks is $N = 131\,072$. Repulsive forces between contacting disks are modeled by linear elastic forces, i.e., $\mathbf{f}_{ij}^{\mathrm{el}} = k(R_i + R_j - r_{ij})\mathbf{n}_{ij}$ for $R_i + R_j > r_{ij}$ and $\mathbf{f}_{ij}^{\mathrm{el}} = \mathbf{0}$ otherwise, where R_i labels the radius of disk i and r_{ij} is the center-to-center distance between the disks i and j. Here, k represents the stiffness and $\mathbf{n}_{ij} \equiv \mathbf{r}_{ij}/r_{ij}$ is the normal unit vector formed from the relative position $\mathbf{r}_{ij} \equiv \mathbf{r}_i - \mathbf{r}_j$. We also add viscous forces to every disk as $\mathbf{f}_i^{\mathrm{vis}} = -\eta\{\mathbf{v}_i - \mathbf{u}(\mathbf{r}_i)\}$, where η, $\mathbf{v}_i$, and $\mathbf{u}(\mathbf{r})$ are the bulk viscosity, velocity of disk i, and external flow field, respectively. Then, we numerically integrate overdamped dynamics [2–4], i.e., $0 = \sum_{j\neq i}\mathbf{f}_{ij}^{\mathrm{el}} + \mathbf{f}_i^{\mathrm{vis}}$, with a time step $\Delta t = 0.1t_0$, where $t_0 \equiv \eta/k$ and the disk velocity is given by $\mathbf{v}_i = \mathbf{u}(\mathbf{r}_i) + \eta^{-1}\sum_{j\neq i}\mathbf{f}_{ij}^{\mathrm{el}}$. In the following, we scale length, time, and stress by $d_0 \equiv (d_L + d_S)/2$, t_0, and k, respectively.

To simulate Kolmogorov flow, we impose external flow fields $\mathbf{u}(\mathbf{r}) = (u_n(y), 0)$ with the x component

$$u_n(y) = A \sin q_n y, \tag{2}$$

where A and $q_n \equiv 2\pi n/L$ $(n = 1, 2, \ldots)$ are an amplitude and wave number, respectively. We use periodic boundary conditions to avoid nonlocal effects due to boundaries [41] and take time averages over the interval $20 \leq At/d_0 \leq 50$, which we have verified to be in steady state [38]. We have examined MD simulations of different system sizes ($L/2$, $L/4$, $L/8$, and $L/16$ with $L \simeq 360d_0$) and confirmed that the results are insensitive to the size (data not shown).

Breakdown of local rheology.—We first examine the local rheology of Kolmogorov flows. Figure 1(a) shows a steady-state flow with $n = 2$. In this figure, force chains (solid lines) develop around nodes of the sinusoidal flow field [Eq. (2)] so that the elastic forces do not vanish and velocities of the disks can deviate from the external flow field. Therefore, the local shear rate $\dot{\gamma}(y)$ is different from $\nabla_y u_n(y) = Aq_n \cos q_n y$ and the stress $\sigma_{xy}(y)$ will show nontrivial local profiles [38] in contrast with studies where the stress profiles are statically determinate [21–23,25,26,28,29].

If the constitutive relations (1) are applicable to inhomogeneous flows, the shear stress $\sigma_{xy}(y)$ must respond to the local shear rate $\dot{\gamma}(y)$ in the same way as σ_{xy}^L. Figure 1(b) shows parametric plots of $\sigma_{xy}(y)$ and $\dot{\gamma}(y)$, where the wave number increases from $n = 1$ to 20 (arrow). The dotted line is the response of σ_{xy}^L, which we consider as the limit of $n = 0$. Clearly, variations of the flow fields are significant and the flow curves are wave-number-dependent. Therefore, the local constitutive relations (1) fail to describe Kolmogorov flow.

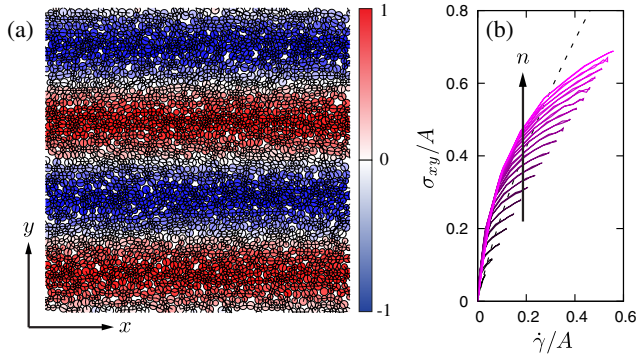

FIG. 1. (a) Snapshot of Kolmogorov flow with wave number $n = 2$. Colors represent the velocity, $-1 \leq v_{ix}/A \leq 1$, and solid lines have width proportional to the elastic forces between the disks (circles). (b) Flow curves obtained from Kolmogorov flow. Lines represent wave numbers increasing from $n = 1$ to 20 (arrow) and the dotted line is given by Eq. (1). In both (a) and (b), $\phi = 0.82$ and $A = 10^{-3}d_0/t_0$ are used.

Particle migration.—What is the origin of the wave number dependence seen in Fig. 1? As suggested by de Cagny *et al.* [32], we now examine the role of particle migration. Figure 2 displays the profiles of (a) velocity $v_x(y)$, (b) shear rate, and (c) shear stress, where the y coordinate is scaled by the wavelength $\lambda_n \equiv L/n$. Increasing the wave number, we find that the velocity

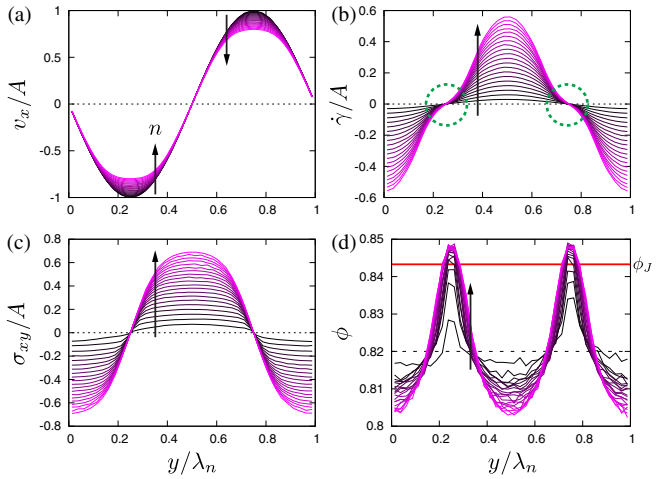

FIG. 2. Profiles of (a) $v_x(y)/A$, (b) $\dot{\gamma}(y)/A$, (c) $\sigma_{xy}(y)/A$, and (d) $\phi(y)$, where A, ϕ, and n are as in Fig. 1(b). Wave numbers increase in the direction of the arrows. Dotted circles in (b) indicate shear localization and the red solid line in (d) represents ϕ_J.

around antinodes is flattened [Fig. 2(a)] and, accordingly, the shear rate becomes small [dotted circles in Fig. 2(b)]; i.e., Kolmogorov flow with high wave numbers exhibits "shear localization." Figure 2(d) shows area fraction profiles that vary significantly in the vicinity of shear localization. Hence, particle migration is indeed present.

To determine if particle migration accounts for wave number dependence in the flow curves, we assume that the local stress is described as $\sigma^L_{xy}(y) = \eta_s[\phi(y), \dot{\gamma}(y)]\dot{\gamma}(y)$ and $\sigma^L_{yy}(y) = \eta_c[\phi(y), \dot{\gamma}(y)]\dot{\gamma}(y)$ and numerically solve the force balance equations

$$\nabla_y \sigma^L_{xy}(y) = -f^{\rm ex}_x(y), \tag{3}$$

$$\nabla_y \sigma^L_{yy}(y) = 0, \tag{4}$$

where $f^{\rm ex}_x(y) = -(4\eta/\pi d_0^2)\phi(y)\{v_x(y) - A\sin q_n y\}$ represents the viscous force acting on the disks [38]. The dotted line in Fig. 3(a) is the measured local shear stress, while the profiles $\dot{\gamma}(y) \equiv \nabla_y v_x(y)$ and $\phi(y)$ are given by the numerical solutions of Eqs. (3) and (4). The local shear stress exhibits discontinuities around the shear-localized regions and significantly deviates from the results of MD simulation [open pentagons in Fig. 3(a)]. The discontinuities are due to the increase of ϕ above ϕ_J in the shear-localized regions [Fig. 2(d)], generating a local yield stress. Because the local model fails even if we take $\dot{\gamma}(y)$ and $\phi(y)$ from simulation data [closed diamonds in Fig. 3(a)] [42], particle migration alone cannot account for the flow curves of Fig. 1(b).

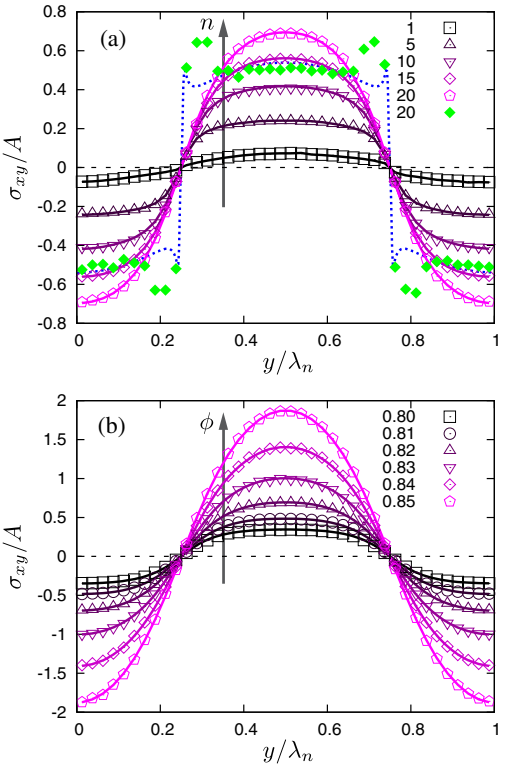

FIG. 3. Stress profiles divided by $A = 10^{-3}d_0/t_0$, where open symbols result from MD simulations and solid lines represent the nonlocal constitutive relations. We increase (a) n and (b) ϕ as listed in the legends and indicated by the arrows, where (a) $\phi = 0.82$ and (b) $n = 20$ are used. Dotted line in (a) is the local constitutive relation $\sigma^L_{xy}(y)$ for $n = 20$, where $\dot{\gamma}(y)$ and $\phi(y)$ are given by numerical solutions of Eqs. (3) and (4). Closed diamonds in (a) represent $\sigma^L_{xy}(y)$ using $\dot{\gamma}(y)$ and $\phi(y)$ from MD simulations.

Nonlocal constitutive relations.—We now formulate nonlocal constitutive relations to describe shear localization and wave-number-dependent flow behavior. We introduce a general nonlocal constitutive relation as

$$\sigma_{xy}(y) = \int dy' \Theta(y, y')\dot{\gamma}(y'), \tag{5}$$

where $\Theta(y, y')$ represents nonlocal shear viscosity. If the system is isotropic, the nonlocal shear viscosity can be normalized as $\Theta(y, y') \equiv \alpha(y - y')\eta_s[\phi(y'), \dot{\gamma}(y')]$, where the propagator $\alpha(l)$ is introduced as a symmetric function of the distance $l \equiv y - y'$ and is normalized as $\int_{-\infty}^{\infty} dl\alpha(l) = 1$ [13]. The shear stress [Eq. (5)] is then given by a weighted integral of the local shear stress, i.e., $\sigma_{xy}(y) = \int dy'\alpha(y - y')\sigma^L_{xy}(y') = \int dl\alpha(l)\sigma^L_{xy}(y - l)$. Because the local model is recovered if the propagator is replaced with Dirac's delta function, i.e., $\sigma_{xy}(y) = \sigma^L_{xy}(y)$ if $\alpha(l) = \delta(l)$, nonlocal effects can be quantified by a finite width of the propagator.

Taking the Fourier transform of Eq. (5), we find that the propagator is given by $\hat{\alpha}(q) = \hat{\sigma}_{xy}(q)/\hat{\sigma}^L_{xy}(q)$, where $\hat{\sigma}_{xy}(q)$ and $\hat{\sigma}^L_{xy}(q)$ are wave-number-dependent Fourier coefficients of the shear stress $\sigma_{xy}(y)$ and local model $\sigma^L_{xy}(y) = \eta_s[\phi(y), \dot{\gamma}(y)]\dot{\gamma}(y)$, which we obtain from the results of MD simulations. Figure 4(a) displays semilogarithmic plots of the propagator (symbols) as a function of the imposed wave number [43]. We see that, if the flow amplitude is small enough, the propagator exhibits a small peak before sharply decreasing (reminiscent of the "dip" in the excess compliance of nonlocal elasticity [36]). Moreover, double-logarithmic plots [Fig. 4(a), inset] imply a linear increase of the propagator for slow flows (dotted line). This result is surprising because the propagator must be symmetric in q_n, and so the presence of a linear term implies that $\hat{\alpha}$ is nonanalytic at zero wave number. For small wave numbers, the propagator can be expanded as

$$\hat{\alpha}(q_n) \simeq \hat{\alpha}(0) + \psi|q_n| - (\xi q_n)^2, \tag{6}$$

where ψ and ξ are introduced as length scales encoding nonlocality. Note that the linear term $\psi|q_n|$ is necessary to capture the peak for slow flows [44]. The solid lines in Fig. 4(a) plot the expansion, Eq. (6), where we establish

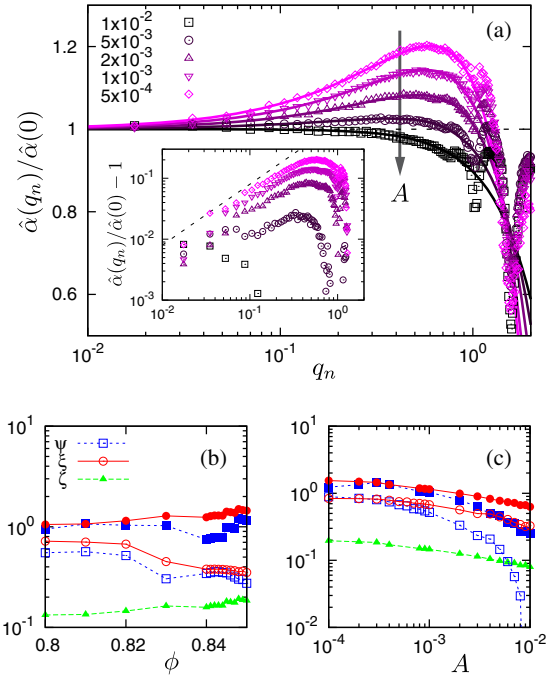

FIG. 4. (a) Semilogarithmic plots of $\hat{\alpha}(q_n)$ for varying A (see legend), where $\phi = 0.82$. Open symbols result from MD simulations, while solid lines are Eq. (6). (Inset) The double-logarithmic plot of $\hat{\alpha}(q_n)/\hat{\alpha}(0) - 1$, where the dotted line has the slope 1. (b),(c) Nonlocal length scales ψ, ξ, and ζ for varying (b) ϕ and (c) A, where (b) $A = 10^{-3} d_0/t_0$ and (c) $\phi = 0.82$ are used. Open symbols are obtained by fitting Eq. (6), while filled symbols are found by fitting the stress profiles with a nonlocal constitutive model.

good agreement with numerical data by adjusting ψ and ξ (see Supplemental Material [38] for the dependence on ϕ).

In previous studies [22–26,28–30], a cooperative length was introduced to represent the range of nonlocality. Because this length depends sensitively on the system's proximity to a jamming or yielding transition, it has been widely accepted that nonlocality has links to critical phenomena. For our systems below jamming, the range of nonlocal effects is quantified by the length scales ψ and ξ, which we have quantitatively estimated by fitting Eq. (6) to numerical results. As shown in Fig. 4(b), these length scales vary little with ϕ and never exceed a few particle diameters for the range of area fractions accessed here. Hence, we find no evidence of a diverging length scale below jamming. In Fig. 4(c), we show that ψ and ξ approach a finite value as the flow amplitude $A \to 0$. Therefore, the nonlocal length scales can reasonably be approximated as constants over a range of ϕ and A near jamming, and we expect Eq. (6) to be transferable to other forms of forcing besides Kolmogorov flow.

Stress profiles.—We demonstrate that the stress profiles from MD simulations can be captured within a nonlocal framework. Inverting Eq. (6) is complicated by the non-analytic term. If we neglect the peak in $\hat{\alpha}$, or if the forcing amplitude is sufficiently large that the peak vanishes, $\psi \simeq 0$, then Eq. (6) can be inverted to obtain $\{1 + (\xi q)^2\}\hat{\sigma}_{xy}(q) \simeq \hat{\sigma}^L_{xy}(q)$. In real space, this nonlocal constitutive relation becomes

$$(1 - \xi^2 \nabla_y^2)\sigma_{xy}(y) \simeq \sigma^L_{xy}(y). \tag{7}$$

Equation (7) is the inhomogeneous Helmholtz equation, where $\sigma^L_{xy}(y)$ plays a role of the "source." Its solution is

$$\sigma_{xy}(y) = \frac{1}{2\xi} \int e^{-\frac{|y-y'|}{\xi}} \sigma^L_{xy}(y') dy'. \tag{8}$$

This is an approximate form of the nonlocal constitutive relation (5), where the propagator $\alpha(l)$ is replaced with the exponential Green function $e^{-(|l|/\xi)}/2\xi$, and ξ is defined as the width of the propagator.

We find that in order to describe stress profiles accurately, Eq. (7) must be generalized to fourth order as $\{1 - \xi^2 \nabla_y^2 + (\xi^4 - \zeta^4)\nabla_y^4\}\sigma_{xy}(y) \simeq \sigma^L_{xy}(y)$, where $\zeta^4 \equiv \int (l^4/4!)\alpha(l) dl$ is the fourth moment of the propagator. In the Supplemental Material [38], we present the solution for the fourth-order propagator, analogous to Eq. (8), along with an approximate method to incorporate the influence of the peak in $\hat{\alpha}$ at low A. As seen in Fig. 3, the stress profiles are in excellent agreement with the nonlocal constitutive relation (solid lines), regardless of the wave number and area fraction, where the profiles $\phi(y)$ and $\dot{\gamma}(y)$, for the source $\sigma^L_{xy}(y) = \eta_s[\phi(y), \dot{\gamma}(y)]\dot{\gamma}(y)$, are provided by MD simulations. Reassuringly, the ϕ and A dependence of the nonlocal fitting parameters [Figs. 4(b) and 4(c), filled symbols] are compatible with the results of fitting Eq. (6) to the propagator.

Summary.—We have studied nonlocal effects in inhomogeneous Kolmogorov flows of soft athermal disks. The rheology is strongly affected by the period of sinusoidal flow fields, and local constitutive relations fail even if particle migration is considered. By introducing a general nonlocal constitutive relation as a convolution of the shear viscosity and strain rate, we quantitatively estimated the range of nonlocality from the propagator. Our method contrasts with fluidity models because the shear viscosity can implement inhomogeneous densities and is more relevant to the jamming transition. Solutions for the stress profiles are in good agreement with simulations, provided the nonanalytic first-order correction is taken into account and the nonlocal constitutive relation is generalized to fourth order—typical diffusion-type models fail to capture profiles for higher wave numbers. Since most models for nonlocal effects [22–26,28–30] or shear bands [45,46] are diffusion type, our approach is an important step towards nonlocal continuum modeling of disordered materials [13]. We find no evidence for critical divergence of the range of nonlocality as jamming is approached from below—nonlocal length scales remain on the order of the particle

diameter for all sampled area fractions and flow rates. We also note that the range of nonlocal *elastic* effects does not diverge under shear (though it does under compression) [36]. As all studies reporting a diverging cooperativity length treated yield stress fluids [16,23–26], our results suggest that such divergence is associated with proximity to yielding, rather than jamming.

We thank K. Baumgarten for fruitful discussions. This work was supported by KAKENHI Grants No. 16H04025 and No. 18K13464 from JSPS. Some computations were performed at the Yukawa Institute Computer Facility, Kyoto, Japan. B. P. T. acknowledges support from the Dutch Organization for Scientific Research (NWO).

*kuniyasu.saitoh.c6@tohoku.ac.jp

[1] D. Bonn, M. M. Denn, L. Berthier, T. Divoux, and S. Manneville, Rev. Mod. Phys. **89**, 035005 (2017).
[2] P. Olsson and S. Teitel, Phys. Rev. Lett. **99**, 178001 (2007).
[3] P. Olsson and S. Teitel, Phys. Rev. Lett. **109**, 108001 (2012).
[4] B. P. Tighe, E. Woldhuis, J. J. C. Remmers, W. van Saarloos, and M. van Hecke, Phys. Rev. Lett. **105**, 088303 (2010).
[5] T. Hatano, J. Phys. Soc. Jpn. **77**, 123002 (2008).
[6] M. Otsuki and H. Hayakawa, Phys. Rev. E **80**, 011308 (2009).
[7] A. Ikeda, L. Berthier, and P. Sollich, Phys. Rev. Lett. **109**, 018301 (2012).
[8] K. Saitoh and H. Mizuno, Soft Matter **12**, 1360 (2016).
[9] K. Baumgarten and B. P. Tighe, Soft Matter **13**, 8368 (2017).
[10] A. H. Clark, J. D. Thompson, M. D. Shattuck, N. T. Ouellette, and C. S. O'Hern, Phys. Rev. E **97**, 062901 (2018).
[11] G. D. R. MiDi, Eur. Phys. J. E **14**, 341 (2004).
[12] P. Jop, Y. Forterre, and O. Pouliquen, Nature (London) **441**, 727 (2006).
[13] A. C. Eringen, *Nonlocal Continuum Field Theories* (Springer Science+Business Media, New York, 2002).
[14] T. Voigtmann, Curr. Opin. Colloid Interface Sci. **19**, 549 (2014).
[15] V. Mansard and A. Colin, Soft Matter **8**, 4025 (2012).
[16] L. Bocquet, A. Colin, and A. Ajdari, Phys. Rev. Lett. **103**, 036001 (2009).
[17] G. Picard, A. Ajdari, F. Lequeux, and L. Bocquet, Phys. Rev. E **71**, 010501(R) (2005).
[18] K. Martens, L. Bocquet, and J.-L. Barrat, Phys. Rev. Lett. **106**, 156001 (2011).
[19] A. Nicolas and J.-L. Barrat, Phys. Rev. Lett. **110**, 138304 (2013).
[20] E. E. Ferrero, K. Martens, and J.-L. Barrat, Phys. Rev. Lett. **113**, 248301 (2014).
[21] O. Pouliquen and Y. Forterre, Phil. Trans. R. Soc. A **367**, 5091 (2009).
[22] J. Goyon, A. Colin, G. Ovarlez, A. Ajdari, and L. Bocquet, Nature (London) **454**, 84 (2008).
[23] K. Kamrin and G. Koval, Phys. Rev. Lett. **108**, 178301 (2012).
[24] D. L. Henann and K. Kamrin, Proc. Natl. Acad. Sci. U.S.A. **110**, 6730 (2013).
[25] K. Kamrin and G. Koval, Comp. Part. Mech. **1**, 169 (2014).
[26] M. Bouzid, M. Trulsson, P. Claudin, E. Clément, and B. Andreotti, Phys. Rev. Lett. **111**, 238301 (2013).
[27] M. Bouzid, A. Izzet, M. Trulsson, E. Clément, P. Claudin, and B. Andreotti, Eur. Phys. J. E **38**, 125 (2015).
[28] P. Jop, V. Mansard, P. Chaudhuri, L. Bocquet, and A. Colin, Phys. Rev. Lett. **108**, 148301 (2012).
[29] P. Chaudhuri, V. Mansard, A. Colin, and L. Bocquet, Phys. Rev. Lett. **109**, 036001 (2012).
[30] G. Katgert, B. P. Tighe, M. E. Möbius, and M. van Hecke, Eur. Phys. Lett. **90**, 54002 (2010).
[31] Z. Tang, T. A. Brzinski, M. Shearer, and K. E. Daniels, Soft Matter **14**, 3040 (2018).
[32] H. de Cagny, A. Fall, M. M. Denn, and D. Bonn, J. Rheol. **59**, 957 (2015).
[33] B. D. Todd, J. S. Hansen, and P. J. Daivis, Phys. Rev. Lett. **100**, 195901 (2008).
[34] M. Schulz, B. M. Schulz, and S. Herminghaus, Phys. Rev. E **67**, 052301 (2003).
[35] M. R. Kuhn, Mech. Mater. **37**, 607 (2005).
[36] K. Baumgarten, D. Vågberg, and B. P. Tighe, Phys. Rev. Lett. **118**, 098001 (2017).
[37] D. J. Durian, Phys. Rev. Lett. **75**, 4780 (1995).
[38] See Supplemental Material at http://link.aps.org/supplemental/10.1103/PhysRevLett.122.188001 for full details, which includes Refs. [39,40].
[39] K. M. Hill and Y. Fan, Phys. Rev. Lett. **101**, 088001 (2008).
[40] Y. Fan and K. M. Hill, New J. Phys. **13**, 095009 (2011).
[41] T. Miller, P. Rognon, B. Metzger, and I. Einav, Phys. Rev. Lett. **111**, 058002 (2013).
[42] The local model agrees with the MD simulations if the wave number is small enough ($n < 3$).
[43] We measure $\hat{\alpha}(q_n) = \hat{\sigma}_{xy}(q_n)/\hat{\sigma}^L_{xy}(q_n)$ for each Kolmogorov flow and plot $\hat{\alpha}(q_n)$ as a function of q_n.
[44] The propagator cannot be described by the analytic fourth-order polynomial, $\hat{\alpha}(q_n) \simeq \hat{\alpha}(0) + (\xi q_n)^2 - (\zeta q_n)^4$, because of its linear dependence on small wave numbers.
[45] S. M. Fielding, Rep. Prog. Phys. **77**, 102601 (2014).
[46] S. M. Fielding, J. Rheol. **60**, 821 (2016).